Int. J. Heat Mass Transfer. Vol. 30, No. 8, pp. 1567–1575, 1987
Printed in Great Britain

0017–9310/87 $3.00 + 0.00
Pergamon Journals Ltd.

Effect of rotation on melting in a horizontal tube rotating about a vertical axis

G. T. GEIGER and E. M. SPARROW

Department of Mechanical Engineering, University of Minnesota, Minneapolis, MN 55455, U.S.A.

(*Received* 11 *November* 1986 *and in final form* 23 *January* 1987)

Abstract—The effect of rotation on the local pattern of melting and on the overall rates of melting and energy storage were determined experimentally for melting in a rotating horizontal tube. The tube was rotated about a vertical axis situated midway between the ends of the tube. Separate sets of experiments were performed for each of two conditions of constraint of the melting solid. In one, the solid was constrained to lie along the axis of the tube, while in the second, the solid was free to fall to the bottom of the tube. For the constrained case, the shape of the melting solid was markedly affected by rotation, but the timewise variations of the melted mass and stored energy were only moderately affected—typically in the 10% range. In the case of the unconstrained solid, the shape of the solid was substantially less affected by rotation than for the constrained case; for the timewise variations of the melted mass and stored energy, the effects of rotation were generally somewhat smaller for the former than for the latter.

INTRODUCTION

THIS IS the second part of a two-part study of melting of a solid contained in a horizontal tube. In the first part, which was reported in ref. [1], the focus of the work was to determine the differences in melting when the solid was constrained not to fall under gravity and when it was free to fall to the bottom of the tube. The experimental results of ref. [1] showed that the rate of melting was very much higher when the solid was unconstrained. For the constrained case, three-dimensional motions were present in the natural convection flow which occurred in the liquid that surrounded the melting solid. The three-dimensional motions were absent in the unconstrained case.

The present experiments are focused on the effect of rotation on the melting of a solid in a horizontal tube. The tube was rotated about a vertical axis situated midway between the ends of the tube. Results were obtained at the highest available rotational speed and compared with those for no rotation, and this comparison indicated that experiments at intermediate rotational speeds were not necessary. The Froude number corresponding to the investigated rotational speed was 4.26, where the radius of rotation which appears in the Froude number was taken as the distance between the axis of rotation and the ends of the tube.

For both the with-rotation and no-rotation cases, melting was initiated and sustained when the wall temperature of the containment tube was rapidly increased to a value above the melting temperature of the encapsulated solid and held constant thereafter. Prior to the temperature increase, the solid was at its melting temperature, and the tube wall was at the same temperature. The phase-change medium used in the experiments was 99% pure n-eicosane paraffin, the melting temperature of which is 36.3°C.

The with-rotation experiments were carried out for three values of the difference between the tube wall temperature and the melting temperature of the solid. The corresponding variation of the Stefan number was from 0.0615 to 0.248. Furthermore, at each fixed value of the temperature difference, separate experiments were performed with the solid constrained to lie along the tube axis and with the solid free to move in response to the prevailing forces. The nature of the experiments was such that for a given rotational condition, temperature difference, and condition of constraint, the time history of the melting was obtained by making a succession of individual melting runs, each of increasingly longer duration. Seven such individual runs were found to be sufficient to define the time history.

Both qualitative and quantitative results will be presented. In the former category are photographs of the residual solid remaining at the end of the melting period. The quantitative results include the timewise variation of the melted mass, of the bulk temperature of the liquid, and of the stored energy. For each of these quantities, comparisons will be made between the with-rotation and the no-rotation results.

The authors are not aware of any prior work either on the effect of rotation on melting in a horizontal tube or on melting in a tube the axis of which is perpendicular to the axis of rotation. Melting in a vertical tube rotating about an axis which coincides with the axis of the tube has been investigated in ref. [2]. The literature survey of ref. [1] for melting in a stationary horizontal tube is also applicable here.

NOMENCLATURE

c	specific heat of liquid	R	inner radius of tube
E_{max}	maximum value of E_{tot}	Ste	Stefan number, $c(T_w - T^*)/\lambda$
E_s	sensible energy stored in liquid melt	T_b	bulk temperature of liquid melt
E_{tot}	sum of E_s and E_λ	T_w	temperature of water bath
E_λ	latent heat needed to melt mass M	T^*	melting temperature
Fo	Fourier number, $\alpha t/R^2$	t	time.
Fr	Froude number, $\omega^2(L/2)/g$		
g	gravity force	Greek symbols	
L	length of tube	α	thermal diffusivity of liquid
M	melted mass	λ	latent heat of melting
M_{tot}	total mass available for melting	ω	rotational speed.

EXPERIMENTS

Aside from the rotation feature, the apparatus for the present experiments is the same as that of ref. [1], so that only a brief description is needed here. The containment tube had internal dimensions of 3.810 and 19.05 cm, diameter and length, respectively, which corresponds to an aspect ratio of 5. The cylindrical portion of the tube was of thin-walled brass (0.318 cm wall thickness), the inner surface of which was highly polished to a mirror finish. At each end, the tube was closed by a Delrin (plastic) disk backed by a 2.54 cm length of closed-pore polystyrene insulation. Each end disk and its backing insulation were part of a Delrin end cap structure which provided positive sealing against leakage.

For the experiments in which the melting solid was unconstrained, the interior-facing surfaces of both end disks were smooth and flat. However, for the experiments in which the solid was constrained, one of the end disks was equipped with a finger-like, 0.635-cm-diameter threaded Delrin rod which extended 3.81 cm into the tube bore.

The tube was supported by a brass shaft which was attached perpendicular to the outside of the cylindrical surface of the tube at a point midway between the ends. In the experimental setup, the axis of the shaft was vertical and the axis of the tube was horizontal, with the shaft extending above the tube. The upper end of the tube support shaft mated with the vertically oriented drive shaft of a variable-speed electric motor via a coupling which allowed connection or disconnection to be accomplished in seconds. With the tube submerged in a water bath, the maximum rotational speed provided by the motor was slightly in excess of 200 rpm. For uniformity, all rotational data runs were made at 200 rpm as measured by a digital tachometer. In the no-rotation runs, the tube was suspended in the same manner as in the rotation runs, except that the motor was not activated.

The tube support shaft also served as a reservoir for receiving the excess volume of liquid paraffin created due to the density decreases which accompany both the solid-to-liquid phase change and the temperature increase of the liquid. To accomplish this storage function, the rod from which the shaft was fabricated was made hollow.

Aside from the containment tube, the other main components of the experimental apparatus were a pair of constant-temperature water baths. One of these baths was used prior to the melting period in order to bring the containment tube and its charge of solid phase-change material to a uniform temperature just below the melting value (36.3°C). The second bath served as the thermal environment of the containment tube during the melting period, with the water temperature maintained at one of three temperature levels, namely, 43.2, 50.2, and 64.1°C. These levels correspond to temperature elevations of 6.9, 13.9, and 27.8°C relative to the melting point. The electric motor from whose shaft the containment tube was suspended overhung the bath. The transference of the containment tube from the first bath to the second bath effectively imposed a step change of temperature on the outside surface of the tube.

To enable fine control of the temperatures of the baths, they were covered at the top and insulated at the sides and bottom. Each bath was equipped with an immersed temperature controller. Temporal and spatial temperature uniformity was achieved to within 0.1°C.

The primary instrumentation included the aforementioned digital tachometer, thermocouples, ASTM-certified precision thermometers, a triple-beam balance, and a calorimeter. The thermocouples were used to measure the wall temperature of the containment tube during selected no-rotation runs, while the precision thermometers served to monitor the constant-temperature baths. Mass measurements were made with the triple-beam balance both before and after each melting run in order to determine the amount of paraffin that had changed phase. The calorimeter was used immediately after each run to measure the bulk temperature of the liquified paraffin.

The experimental procedure for a given run can be subdivided into a pre-melting stage, the melting

period, and a post-melting stage. In the pre-melting stage, a void-free, flat-ended, tube-filling cylinder of solid paraffin was cast in place in the containment tube, after which the tube and its contents were weighed and then brought to the melting temperature in the first constant-temperature bath. During this stage, the temperature of the second bath was brought to the desired value and, as a final task, the drive motor was warmed up, if a rotational run was in the offing.

The transference of the containment tube to the second constant-temperature bath and its coupling to the motor shaft was accomplished in about 10 s, and an additional 5 s was required to attain the desired rotational speed (200 rpm) from start-up. During the melting period, the speed was checked periodically with the tachometer and corrected if necessary. Also, the calorimeter was prepared for use subsequent to the end of the run. About 15 s before the end of the run the motor speed control was set to zero in anticipation of the coast-down period and the time required to decouple the containment tube from the motor shaft.

After the run, the tube was taken from the constant-temperature bath, opened at one end, and the remaining solid extracted. The liquid was then poured into the calorimeter and its bulk temperature determined. Then, the extracted solid was wiped free of any adhering liquid and weighed. If the solid was earmarked for subsequent photography, it was set aside; if not, it was returned to the paraffin storage receptacle along with the liquid from the calorimeter. As a final step, all portions of the apparatus were thoroughly cleaned to eliminate all traces of paraffin.

PATTERNS OF MELTING

The rotation of the containment tube gave rise to two additional forces which acted on the fluid particles in the liquid melt—the centrifugal and Coriolis forces. These forces altered the pattern of fluid flow in the melt relative to that in the stationary case. The altered flow pattern is expected to change the pattern of melting, especially when the primary path for heat transfer from the tube wall to the melting front is through the liquid melt.

Photographs of the residual solid remaining at the end of the melting period are presented in Figs. 1–3 for the with-rotation case. All of these photographs correspond to the intermediate temperature difference, 13.9°C, between the water bath and the melting point of the paraffin ($Ste = 0.124$). Figures 1 and 2 are longitudinal views which correspond respectively to the solid either constrained or unconstrained during the melting period, while Fig. 3 shows end views for the respective cases. Photographs of the residual solid for the no-rotation case have been presented in Figs. 2 and 3 of ref. [1], and the key features of those photographs will shortly be compared with those of the present Figs. 1–3.

Figures 1(a) and (b) correspond to melting periods of 11.8 and 20.7 min, respectively. Both photographs are of the bottom of the solid. When viewed from below, the direction of rotation is counterclockwise. From Fig. 1(a), it is seen that there is less melting at the ends of the solid than away from the ends. Also, ridges appear to have formed in the near-end regions on the leeward side of the solid. At a later time, Fig. 1(b), the disparity in the amount of melting at and away from the ends has become more marked, and the aforementioned ridges have developed into flats. The typical end view of the constrained, melting solid, Fig. 3(a), is very nearly a perfect circle centered on the axis of the tube.

The just-displayed, partially melted, constrained solids for the with-rotation case differ markedly from those for the no-rotation case [1]. In particular, for the latter, there was no significant difference between the shape of the solid at and away from the ends. Furthermore, the bottom of the solid was characterized by nearly *periodic* undulations consisting of successive peaks and valleys, suggesting the presence of a cellular, periodic, three-dimensional natural convection flow in the lower part of the containment tube. The top of the solid was smooth and uniform over its entire length, indicating a two-dimensional natural convection flow in the upper part of the containment tube. The end-view photograph showed the solid to be non-circular in cross-section.

Attention will now be turned to the unconstrained solid. In this case, the solid is situated adjacent to the lower wall of the containment tube, with only a thin liquid-filled gap separating the solid from the wall. The thermal resistance for heat flow across the gap is smaller than that for convective heat flow between the upper portion of the solid and the upper wall of the tube. As a consequence, the nature of the convective motions should play a lesser role for the melting of the unconstrained solid than for the constrained solid.

Figures 2(a) and (b) are longitudinal views looking down at the top of the unconstrained solid at melting times of 7.4 and 13.3 min, respectively. When viewed in this direction, the rotation of the containment tube is clockwise. As was also true in the constrained case, Fig. 2 shows that ridges form on the leeward side of the solid adjacent to the ends and that subsequently the ridges develop into flats. However, in contrast to the constrained case, there is very little difference in the amount of melting at and away from the ends. This finding is consistent with the expected lesser role played by the convective heat transfer. The end-view photograph shows the lens shape that is characteristic of the unconstrained melting mode.

Blemishes in the surface of the mid-section of the solid can be seen in Fig. 2. These blemishes are altogether extraneous and are related to the aperture in the tube wall at the point where the wall is interconnected to the support shaft.

A comparison of the present with-rotation photographic results for the unconstrained solid with those

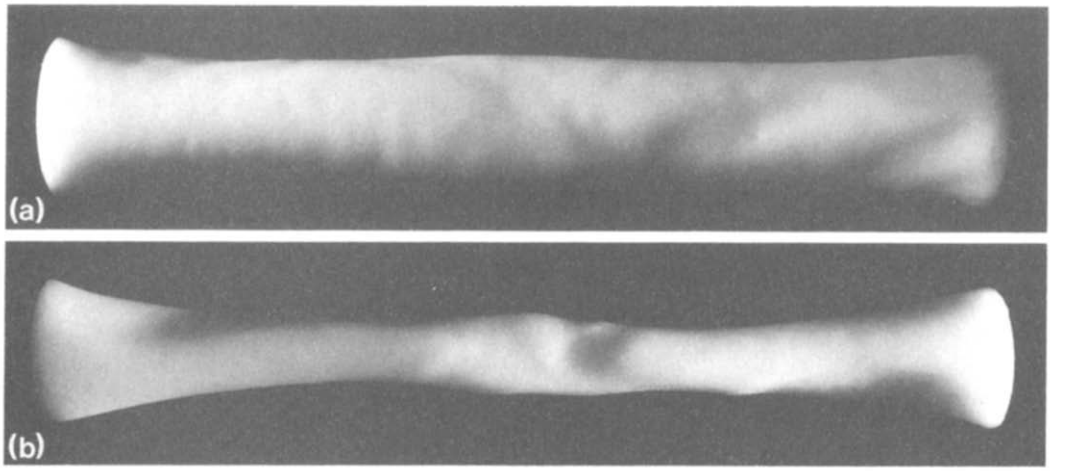

FIG. 1. Longitudinal views of the constrained melting solid.

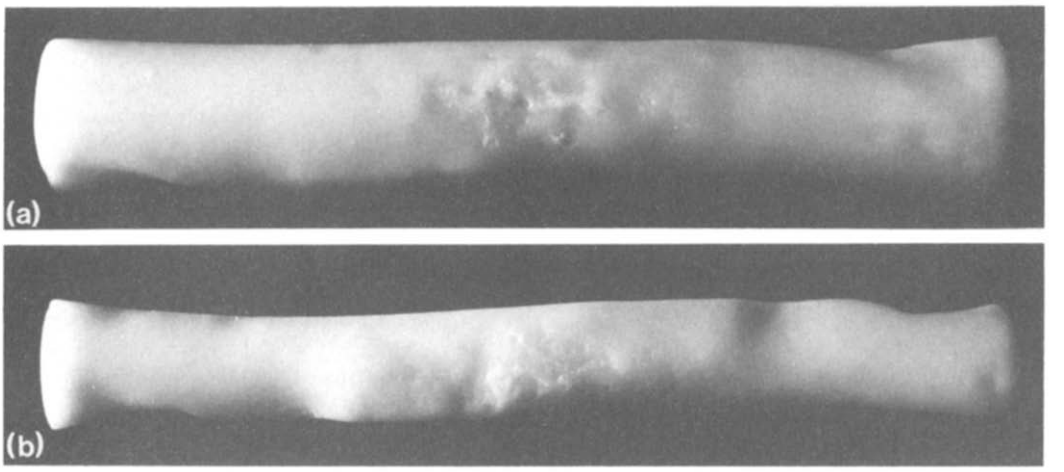

FIG. 2. Longitudinal views of the unconstrained melting solid.

for no rotation [1] indicates differences that are relatively minor. For one thing, the end views show the same lens-like cross-section for both with and no rotation. The longitudinal views differ in that for the no-rotation case, the shape of the solid is strictly uniform all along its length, while with rotation there are moderate lengthwise nonuniformities plus the aforementioned end-adjacent flattening.

The factors which influence the pattern of fluid flow in the presence of rotation will now be considered. As noted earlier, the rotation-related forces are the centrifugal and Coriolis forces. The former acts outward along the line connecting a fluid particle with the center of rotation. The Coriolis force acts perpendicular to both the angular velocity vector and the direction of relative motion.

The centrifugal forces cause cooler, relatively denser fluid to be displaced away from the axis of rotation (i.e. toward the ends of the tube), with a consequent flow of hotter, relatively less-dense fluid toward the axis of rotation (i.e. toward the mid-region of the tube). These fluid motions tend to give rise to enhanced melting in the mid-region of the solid and diminished melting near the ends. As noted earlier, this tendency is more strongly manifested when the solid is constrained.

The aforementioned flow pattern induced by the centrifugal forces is modified by the Coriolis forces. In particular, the flow of hotter, relatively less-dense fluid toward the axis of rotation is deflected toward the windward side of the containment tube. As the fluid washes over the leeward side en route to the windward side, it causes increased melting at the former.

The centrifugally induced motions along the axis of the containment tube appear to be of sufficient strength to break up the cellular, periodic flow which prevailed in the portion of the tube beneath the constrained solid when there was no rotation.

Diagrams conveying conjectured flow patterns for constrained and unconstrained melting are presented in Figs. 4(a) and (b). Attention is called to the end-adjacent recirculation zones which are responsible for increased melting on the leeward side.

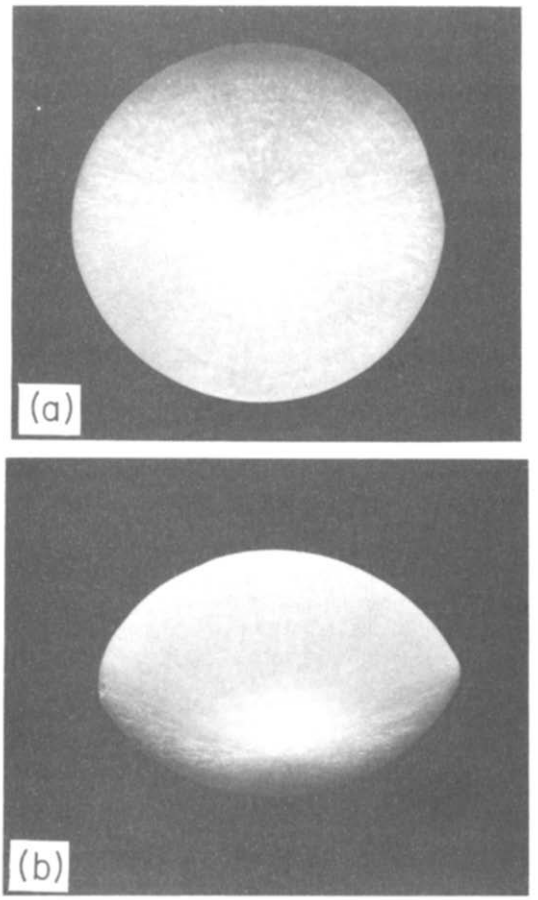

FIG. 3. End views of (a) the constrained and (b) the unconstrained melting solids.

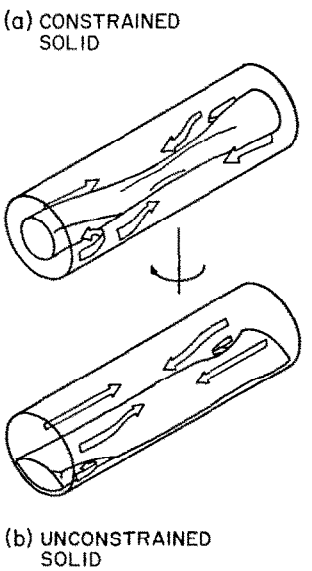

FIG. 4. Conjectured flow patterns about (a) the constrained and (b) the unconstrained melting solids.

MELTED MASS AND STORED ENERGY

In the presentation which follows, quantitative results will be given for the timewise variation of the melted mass and the stored energy.The duration t of the melting period, which serves as the independent variable, will be expressed in dimensionless terms via the Fourier–Stefan product, as suggested by heat conduction theory. The definitions of the Fourier and Stefan numbers to be used here are

$$Fo = \alpha t/R^2, \quad Ste = c(T_w - T^*)/\lambda \qquad (1)$$

where the thermophysical properties α and c are those of the liquid melt, evaluated here at the melting temperature T^*. The characteristic dimension in the Fourier number is the radius R of the bore of the containment tube.

In addition to its involvement in the representation of the dimensionless time *Fo Ste*, the Stefan number will also be used as a parameter to represent the characteristic temperature difference of the problem. As seen in equation (1), that temperature difference involves the water-bath temperature T_w and the melting temperature T^*. For the three values of $(T_w - T^*)$ used in the experiments, namely, 6.9,13.9, and 27.8°C, the corresponding values of *Ste* are 0.0615, 0.124, and 0.248.

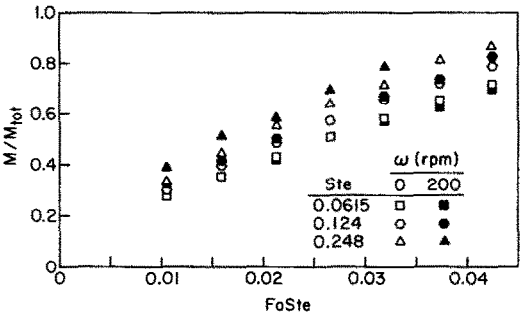

FIG. 5. Melted mass results for the case of the constrained solid.

Melted mass

The mass melted between $t \doteq 0$ and t will be denoted by M, while the total mass in the containment tube that is available for melting is M_{tot}. The experimental results for the timewise variation of the melted mass will be presented as the M/M_{tot} ratio plotted as a function of *Fo Ste* for parametric values of *Ste*.

The melted mass results for the constrained solid are presented in Fig. 5. In the figure, the open symbols represent the no-rotation data while the black symbols are the with-rotation data. As explained earlier, all of the with-rotation experiments were carried out at the highest available rotational speed of 200 rpm ($Fr = 4.26$). At all times except the two largest times, M/M_{tot} data were obtained with and without rotation for all three values of *Ste*, so that there are six data points at each *Fo Ste*, although not all can be seen due to overlap. However, at $Ste = 0.248$, M/M_{tot} could not be determined at the two largest times because the solid had split at the necked-down region adjacent to the center of rotation (Fig. 1), so that the black triangles are absent.

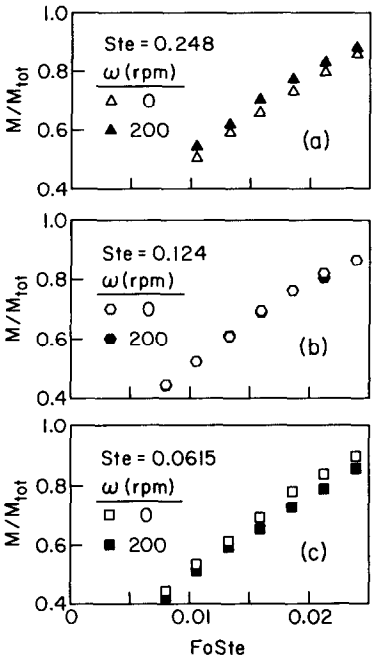

FIG. 6. Melted mass results for the case of the unconstrained solid.

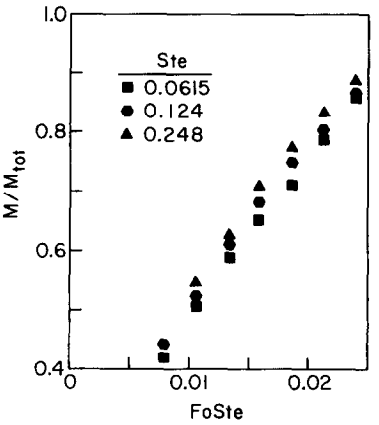

FIG. 7. Stefan number ordering of the with-rotation melted mass results for the case of the unconstrained solid.

An overall inspection of Fig. 5 indicates that the effect of rotation on the melted mass is moderate and is of different sign depending on the Stefan number. At the highest Stefan number, rotation gives rise to a 6–15% increase in melting. On the other hand, at the smallest Stefan number, rotation brings about a slight decrease in melting, with the largest decrease being about 5%. The fact that the rotation-related effects are moderate despite the significant changes in the pattern of melting may be rationalized by noting that rotation enhances melting away from the ends of the solid and diminishes melting adjacent to the ends. It is these counteracting tendencies that moderate the net effect. At the largest *Ste*, the away-from-end changes are greater than the end-adjacent changes, with an opposite relationship at the smallest *Ste*.

Due to these differing rotational effects at various Stefan numbers, the sensitivity of M/M_{tot} to *Ste* is greater when rotation is present than when there is no rotation.

For the unconstrained solid, the M/M_{tot} results are presented in a format somewhat different from Fig. 5 to avoid overlap due to a relatively weak dependence of the data on *Ste*. In Fig. 6, M/M_{tot} for the unconstrained case is plotted as a function of *Fo Ste* in three separate graphs, one for each *Ste*. Inspection of Fig. 6 shows that the effects of rotation on the melting of an unconstrained solid are qualitatively the same as those already identified for a constrained solid—an increase in melting at the largest *Ste* and a decrease at the smallest *Ste*. The increases lie in the range of 3–8% and are, therefore, smaller than those encountered for the constrained case. The decreases are also in the 3–8% range, which are, surprisingly, somewhat greater than the decreases for the constrained solid.

On the basis of the earlier discussion and the photographic presentation of Figs. 1–3, it might have been expected that the melted mass results would be less affected by rotation when the solid is unconstrained. This appears not to be necessarily the case, suggesting that the conflicting tendencies for increased melting away from the ends and decreased melting adjacent to the ends may be trading off differently for the constrained and unconstrained cases.

The ordering of the M/M_{tot} results with *Ste* is conveyed in Fig. 7 for the unconstrained solid in the presence of rotation. The figure shows that at a given dimensionless time, M/M_{tot} increases with increasing *Ste*. This ordering is the same as that of Fig. 5 for the constrained case where, in fact, it is in evidence for both the with-rotation and no-rotation operating conditions. It is, however, interesting to note from Fig. 7 of ref. [1] that for the unconstrained solid in the absence of rotation, M/M_{tot} increases slightly with decreasing *Ste*, which is just opposite to the trend in evidence in Fig. 7. Thus, rotation reverses the *Ste* dependence of the M/M_{tot} results for the unconstrained solid.

Literature information on rotation effects

As noted earlier, a literature search failed to reveal any prior information on the effect of rotation on melting in a horizontal tube or in a tube whose axis is perpendicular to the axis of rotation. The only investigated situation involving melting in the presence of rotation appears to be the vertical tube rotating about its own (vertical) axis [2]. In that case, it was found that rotation gave rise to substantially increased rates of melting for all Stefan numbers. This is to be contrasted with the present results which show a moderate effect of rotation on the rate of melting and a Stefan-number dependence of the sign of the effect. Clearly, the rotational effect is highly configuration dependent.

To gain broader perspective, the literature was examined to identify the effect of rotation on natural

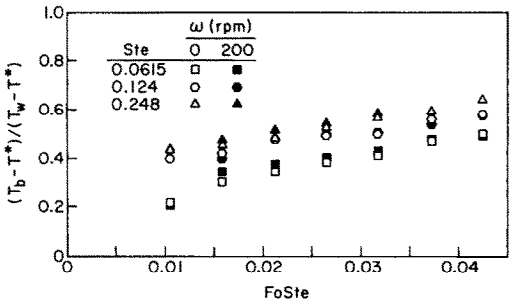

FIG. 8. Liquid-melt bulk temperatures for the case of the constrained solid.

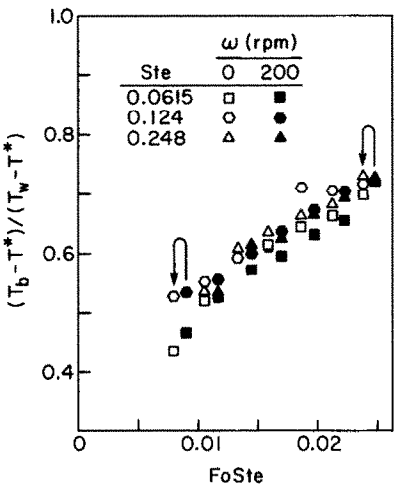

FIG. 9. Liquid-melt bulk temperatures for the case of the unconstrained solid.

convection in the absence of phase change. The configuration of particular interest was a horizontal annulus rotating about a vertical axis, since it approximated the physical situation encountered in the present experiments. No results were found for this case, so that it was necessary to consider other configurations.

For the vertical annulus rotating about its own axis, rotation was found either to decrease the heat transfer [3, 4], increase the heat transfer [5], or sequentially decrease and increase the heat transfer [6] as the rotational speed increased. These differing tendencies may reflect differences in the thermal and hydrodynamic boundary conditions. Another commonly investigated configuration is a horizontal layer heated from below and rotating about a vertical axis. For this case, rotation caused either a decrease in the heat transfer [7, 8] or a sequential increase and decrease [7–9].

The foregoing survey indicates that the different effect of rotation on the present melting results and those of ref. [2] fits into the larger picture where rotation affects natural convection heat transfer in a nonuniform manner.

Bulk temperature of liquid melt

The energy stored in the phase-change medium during the melting period is the sum of the energies used to supply the latent heat of melting and to increase the sensible heat of the liquid melt. The evaluation of the latter requires the bulk temperature T_b of the liquid, measurements of which were made at the end of each melting experiment.

The bulk temperature data for constrained and unconstrained melting are respectively presented in Figs. 8 and 9. In each figure, open and black symbols are used to represent the no-rotation and with-rotation results. Each figure also includes all three investigated Stefan numbers. To avoid overlap, the with-rotation data of Fig. 9 have been shifted slightly to the right of their proper abscissa locations. In reality, the no-rotation and with-rotation data fall at common values of the abscissa. On the ordinate, the bulk temperature is embedded in the dimensionless group $(T_b-T^*)/(T_w-T^*)$.

In all cases, the bulk temperature increases with time, but the increase is moderated because the melting process continually supplies additional liquid at T^* (the lowest temperature in the system) to the melt. In general, the bulk temperature is quite insensitive to the presence or absence of rotation, and the small differences which do occur are somewhat obscured by data scatter. For the constrained case (Fig. 8), there is a slight tendency for rotation to increase the bulk temperature. In the case of the unconstrained solid (Fig. 9), the data for the lowest Stefan number are most affected by rotation, but not in a consistent manner. Note that the data scatter in Figs. 8 and 9 is somewhat more pronounced than that in Figs. 5–7, reflecting the greater difficulty of the bulk temperature measurement.

The bulk temperatures for the unconstrained case exceed those for the constrained case. This behavior has already been rationalized in ref. [1].

Stored energy

The energy stored in the phase-change medium during the time interval between $t = 0$ and t will be denoted by E_{tot}, while the latent heat and sensible heat contributions to E_{tot} are E_λ and E_s, so that

$$E_{tot} = E_\lambda + E_s. \tag{2}$$

Since M is the amount of mass melted between $t = 0$ and t, it follows that

$$E_\lambda = \lambda M. \tag{3}$$

Furthermore

$$E_s = M\int_{T^*}^{T_b} c\,\mathrm{d}T = M\bar{c}(T_b - T^*). \tag{4}$$

Since $c(T)$ for n-eicosane can be represented as a linear function [10], $\bar{c}$ corresponds to $c(T)$ at $(T_b+T^*)/2$.

A comparison between E_s and E_λ is made in Fig. 10 for all of the operating conditions employed here and

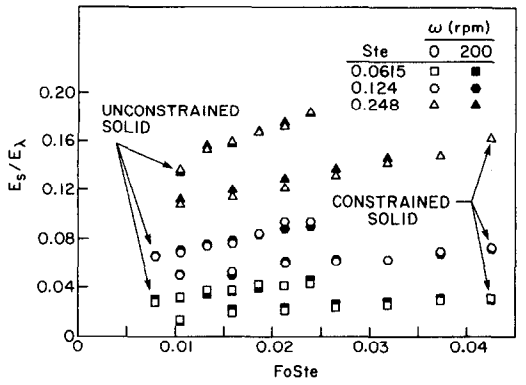

FIG. 10. Comparison of energy stored due to sensible heat and latent heat effects.

in ref. [1]. In the figure, the E_s/E_λ ratio is plotted vs *Fo Ste* for parametric values of *Ste* and of the rotational speed ω, and for the two conditions of constraint. Among the three parameters, the data are most responsive to *Ste*, secondmost responsive to the condition of constraint, and least responsive to the rotational speed. The ordering of the data with *Ste* is as expected since this dimensionless group is a measure of sensible to latent heat storage. The higher E_s/E_λ values for the unconstrained mode reflect the higher liquid bulk temperatures that were noted in connection with Figs. 8 and 9. For the most part, the effect of rotation on E_s/E_λ did not exceed 5%.

The results for E_{tot} will now be presented. For the presentation, it is convenient to use the dimensionless ratio E_{tot}/E_{max}, where E_{max} is the maximum value of E_{tot} for each operating condition. E_{max} is achieved when all of the solid has melted and when the liquid melt has attained a uniform temperature equal to T_w. Therefore

$$E_{max} = \lambda M_{tot} + M_{tot}\bar{c}(T_w - T^*) \quad (5)$$

where $\bar{c}$ now corresponds to $(T_w + T^*)/2$. Note that for a given thermal operating condition, E_{max} is the same in the presence and in the absence of rotation. Therefore, with regard to the effect of rotation, comparisons of E_{tot}/E_{max} are equivalent to comparisons of E_{tot} itself.

The E_{tot}/E_{max} results are plotted as a function of time in Figs. 11 and 12, respectively, for the constrained and unconstrained solids. Each figure contains data for both no-rotation and with-rotation operation at all of the three investigated Stefan numbers.

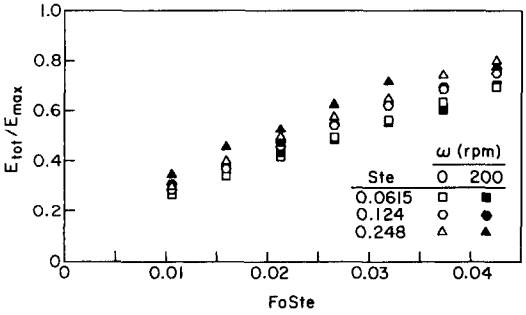

FIG. 11. Results for the total stored energy for the case of the constrained solid.

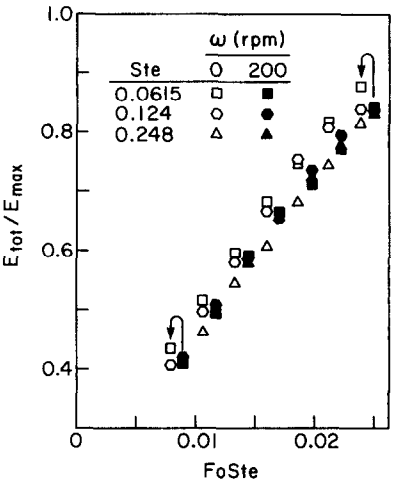

FIG. 12. Results for the total stored energy for the case of the unconstrained solid.

An examination of Fig. 11 (constrained case) indicates that at the highest *Ste*, there is a definite increase in E_{tot} due to rotation, with the increase ranging from 6 to 16%. At the intermediate *Ste*, an increase is still in evidence, but it is smaller. On the other hand, at the lowest *Ste*, the rotation effect is not uniform with time and is relatively small. Overall, the E_{tot}/E_{max} data are more sensitive to *Ste* in the presence of rotation than when there is no rotation. These trends are similar to those for M/M_{tot} as discussed in connection with Fig. 5.

The with-rotation data of Fig. 12 (unconstrained case) have been shifted to avoid overlap, as indicated in the figure. Rotation acts to increase E_{tot}/E_{max} at the highest *Ste* (by 2–7%) and to decrease E_{tot}/E_{max} at the lowest *Ste* (by 1–6%). Again, this behavior mirrors that of M/M_{tot}. It is also seen from Fig. 12 that E_{tot}/E_{max} is less sensitive to *Ste* in the presence of rotation.

From the foregoing, it is evident that rotation affects E_{tot}/E_{max} differently depending upon whether the solid is constrained or unconstrained.

CONCLUDING REMARKS

The experiments reported here constitute the first study of melting in a horizontal tube which rotates about a vertical axis and, in general, of melting in a tube whose axis is perpendicular to the axis of rotation. Separate sets of experiments were performed in which (a) the melting solid was constrained to lie along the tube axis and (b) the solid was free to fall to the bottom of the tube. The characteristic temperature difference for melting was varied so as to yield variations in the Stefan number from 0.0615 to 0.248.

For the constrained case, the shape of the melting solid was markedly affected by rotation such that there was considerably more melting away from the ends of the solid than near the ends. Despite this,

global quantities such as the timewise variations of the melted mass and of the stored energy were only moderately affected by rotation, typically in the 10% range. In the case of the unconstrained solid, the shape of the solid was substantially less affected by rotation than for the constrained case; for the timewise variations of the melted mass and stored energy, the effects of rotation were generally somewhat smaller for the former than for the latter.

The rotational effects encountered here were substantially smaller than those for melting in a vertical tube rotating about its own (vertical) axis.

REFERENCES

1. E. M. Sparrow and G. T. Geiger, Melting in a horizontal tube with the solid either constrained or free to fall under gravity, *Int J. Heat Mass Transfer* **28,** 1007–1019 (1986).
2. A. Chaboki and E. M. Sparrow, Melting in a vertical tube rotating about a vertical, colinear axis, *Int. J. Heat Mass Transfer* **30,** 613–622 (1987).
3. F. Kreith, Convection heat transfer in rotating systems, *Adv. Heat Transfer* **5,** 129–251 (1968).
4. M. Bowden and H. F. Eden, Thermal convection in a rotating fluid annulis, *J. Atmos. Sci.* **22,** 185–195 (1965).
5. G. M. Homsy and J. L. Hudson, Centrifugally driven thermal convection in a rotating cylinder, *J. Fluid Mech.* **35,** 33–52 (1969).
6. D. Tang and J. L. Hudson, Experiments on a rotating fluid heated from below, *Int. J. Heat Mass Transfer* **26,** 943–949 (1983).
7. H. T. Rossby, A study of Bénard convection with and without rotation, *J. Fluid Mech.* **36,** 309–335 (1969).
8. J. C. Morgan, Nonlinear Bénard convection with rotation, *J. Fluid Mech.* **57,** 433–458 (1973).
9. C. Hunter and N. Riahi, Nonlinear convection in a rotating fluid, *J. Fluid Mech.* **72,** 433–454 (1975).
10. E. I. Griggs and W. R. Humphries, A design handbook for phase change thermal control and energy storage devices, NASA Technical Paper 1074 (1977).

EFFET DE LA ROTATION SUR LA FUSION DANS UN TUBE HORIZONTAL TOURNANT AUTOUR D'UN AXE VERTICAL

Résumé—L'effet de la rotation sur la configuration locale de la fusion et sur les vitesses de fusion et de stockage d'énergie est déterminé expérimentalement pour la fusion dans un tube horizontal qui tourne autour d'un axe vertical situé à mi-distance des extrémités du tube. Des séries séparées d'expériences sont faites pour chacune des deux conditions de contrainte sur le solide en fusion. Dans l'une, le solide est obligé de rester le long de l'axe du tube, tandis que dans l'autre le solide est libre de tomber à la base du tube. Pour le premier cas, la forme du solide en fusion est nettement affectée par la rotation, mais les variations dans le temps de la masse fondue et de l'énergie stockée sont faiblement modifiées, typiquement de l'ordre de 10%. Dans le cas du solide libre, la forme du solide est nettement moins affectée par la rotation que dans le premier cas; pour les variations dans le temps de la masse fondue et de l'énergie stockée, les effets de la rotation sont généralement un peu plus faible pour le dernier cas.

AUSWIRKUNG DER ROTATION AUF DAS SCHMELZVERHALTEN IN HORIZONTALEN ROHREN, DIE SICH UM EINE VERTIKALE ACHSE DREHEN

Zusammenfassung—Der Einfluß der Rotation auf die Schmelzform und auf den zeitlichen Verlauf des Schmelzens und der Energiespeicherung wurde experimentell für die Schmelzvorgänge in rotierenden, horizontalen Rohren bestimmt. Das Rohr rotiert um eine vertikale Achse, die in der Mitte der beiden Rohrenden liegt. Die Versuche wurden unter den folgenden Bedingungen durchgeführt: Im ersten Fall wurde der Feststoff axial im Rohr gehalten, während er im zweiten Fall frei auf den Rohrboden fallen konnte. Im Falle der Befestigung beeinflußte die Rotation dessen Form nennenswert, während die zeitliche Veränderung der Schmelzmasse und der gespeicherten Energie nur mäßig beeinflußt wurden—typischerweise im 10%-Bereich. Ohne Befestigung wurde die Form des Schmelzkörpers durch die Rotation wesentlich weniger beeinflußt als mit Befestigung; für die zeitliche Veränderung der Schmelzmasse und der gespeicherten Energie sind die Einflüsse der Rotation im allgemeinen im ersten Fall etwas geringer als im zweiten.

ВЛИЯНИЕ ВРАЩЕНИЯ НА ПЛАВЛЕНИЕ В ГОРИЗОНТАЛЬНОЙ ТРУБЕ, ВРАЩАЮЩЕЙСЯ ВОКРУГ ВЕРТИКАЛЬНОЙ ОСИ

Аннотация—Экспериментально изучено влияние вращения на локальные характеристики плавления, а также на общую интенсивность плавления и величину поглощенной энергии при вращении горизонтальной трубы около вертикальной оси, расположенной посередине между ее концами. Для каждого из условий фиксации плавящегося твердого тела проводились отдельные серии экспериментов. При первом условии тело жестко фиксировалось вдоль оси трубы, а при втором могло свободно перемещаться на дно трубы. В случае жесткой фиксации вращение заметно влияло на форму плавящегося твердого тела, но величина зависимости расплавленной массы и накопленной энергии от времени изменялась при этом весьма незначительно, примерно на 10%. При свободном перемещении форма твердого тела значительно меньше подвергалась влиянию вращения, чем в случае жесткой фиксации. Влияние вращения на зависимость расплавленной массы и накопленной энергии от времени в первом случае, в общем, была меньше, чем во втором.